

# TEST BENCH DEVELOPMENT AND IMPLEMENTATION FOR EXPERIMENTAL DETERMINATION OF MECHANICAL LOSSES IN SINGLE CYLINDER INTERNAL COMBUSTION ENGINES

*Carlos Alberto Romero Piedrahita*  
*Department of Technologies<sup>1</sup>*

*Mauricio Monroy Jaramillo*  
*Department of Mechanical Engineering<sup>1</sup>*

*Juan David Ramírez Alzate*✉  
*Department of Mechanical Engineering<sup>1</sup>*  
*juandaviramireza@utp.edu.co*

<sup>1</sup>*Universidad Tecnológica de Pereira*  
*10-27, Cra 27, Pereira, Colombia, 660003*

✉Corresponding author

## Abstract

As mechanical efficiency has great relevance in the alternative engine performance, the authors research in the development of testing facilities to characterize the sources of engine mechanical losses. The present paper deals with the realization of a hardware platform to conduct experimental studies in small combustion engines to experimentally characterize the mechanical losses of a single-cylinder internal combustion engine by means of the indicated diagram and motoring methods. The system was completed by means of an electrical motor-generator coupled to a single-cylinder air-cooled spark ignition engine, a self-developed electronic hardware control, and a PC-based instrumentation and data acquisition system. Specifications of load-motoring-starting system, including the description of the proprietary electronic load regulation system, are detailed. Also, the instrumentation system of in-cylinder and intake pressures; Temperatures of intake air, exhaust gases, lubricant oil, and engine block; effective torque and crankshaft position are described, including the signal acquisition system. The methodologies for indicated diagram and motoring method are described, mentioning the required measurements to apply each method and the engine load-temperature considerations when an engine is tested in fired or motored conditions. The platform was used to study the mechanical losses of the engine under motored and fired conditions under a wide range of rotational speeds and throttle openings, allowing to draw conclusions about the operating features of the developed test bench in itself, and also about the mechanical losses of the engine tested. Initially, samples of cylinder pressure, torque, intake pressure as function of crank angle and indicate diagram were obtained, showing similar waveforms present in related literature. Then, variations of the aforementioned temperatures against rotation speed and throttle opening and results for the mechanical losses determined by indicated diagram and motoring methods are shown. Finally, two empirical correlations are proposed to estimate the mechanical losses. In the future the hardware platform will be utilized to investigate in-cylinder engine parameters, detailed thermal and mechanical engine performance.

**Keywords:** internal combustion engine, test bench, mechanical losses, experimental determination, indicated and motoring methods.

DOI: 10.21303/2461-4262.2023.002847

## 1. Introduction

Due to the technological evolution of internal combustion engines (ICE) and the variety of designs, geometries, materials and surface treatments of components, lubricants, additives and fuels used to improve the engine performance, it is necessary to have test stations to identify the different operating characteristics of ICE and evaluate the effects that the different technological alternatives have on the effective, indicated or mechanical performance [1, 2].

ICE test benches usually integrate the load and/or motoring system, which is mechanically coupled to the tested engine. Load systems may use different technologies, including friction braking systems, hydraulic systems, electric motor-generator drive [3] and electromagnetic [1, 4–6]. On the other hand, as motoring systems, direct current or alternating current electric motors are usually used [7].

A purpose of the engine test benches is the characterization of the effective and the indicated performance (torque, power, specific fuel consumption, net efficiency, indicated work). That cha-

racterization is required to determine the overall engine mechanical losses. When more detailed mechanical losses assessment is needed, test rigs such as rotating or reciprocating tribometers are used to evaluate the performance of individual systems and/or mechanisms [8–11], or test mockups are built to isolate the mechanism or auxiliary system concerned [9, 12–15].

Related to mechanical losses, these are composed by the rubbing friction of all the moving pairs, the pumping work due to the intake and exhaust process backpressure and the power needed to drive the auxiliary systems [16–21]. Only the friction losses consume 4–15 % of the energy provided by the fuel [8], i.e., that by reducing the mechanical loss is possible to improve the net engine efficiency. Therefore, it is important to rely on experimental engine test benches to quantify the detailed and overall mechanical losses, as well as to assess the effects the lubrication modifiers, properties of the materials, and the surface finishing of engine contacting pairs have on the engine rubbing friction and wear.

The objective of the present paper is the integration of a test bench for starting, motoring, and loading of an internal combustion engine for the purpose of scientific and academic exploitation on overall engine performance assessment, and particularly on the experimental studies of engine mechanical losses.

The test rig presented in this paper has been developed to determine the mechanical losses of low power (less than 2.5 kW) internal combustion engines through the indicated diagram and motoring methods. The test rig uses an electrical machine that can operate as needed as starter motor, motoring device and variable brake for the ICE in fired condition. The load-motoring system can also be used to determine external performance characteristics of a complete engine and to diagnose abnormal mechanical losses and with them assessing the technical condition of the engine.

The following sections detail the test bench, describing the main structure and presenting the specifications of the test engine, the load system, the instrumentation and the data acquisition system. Special attention has been given to the development or the electronic circuit of the load regulation system. The test methodologies applicable to the test bench are presented. Crank angle, cylinder pressure, torque, intake pressure and temperatures at engine block, intake manifold, exhaust pipe and oil plug were measured and the obtained results of the mechanical losses by means of the indicated diagram and drag methods are presented graphically. Two empirical correlations to estimate the mean effective pressure of mechanical losses of the engine tested as a function of the rotational speed and the throttle valve opening are found.

## 2. Materials and methods

### 2.1. Methodological scheme of the test bench integration

This section presents the components and the integration process of the test bench including the description of the bench structure, the tested internal combustion engine, the load-motoring system, the instrumentation, and the data acquisition system. The integration scheme of the test bench is presented in Fig. 1. Finally, two of the applicable mechanical losses' determination methods are described.

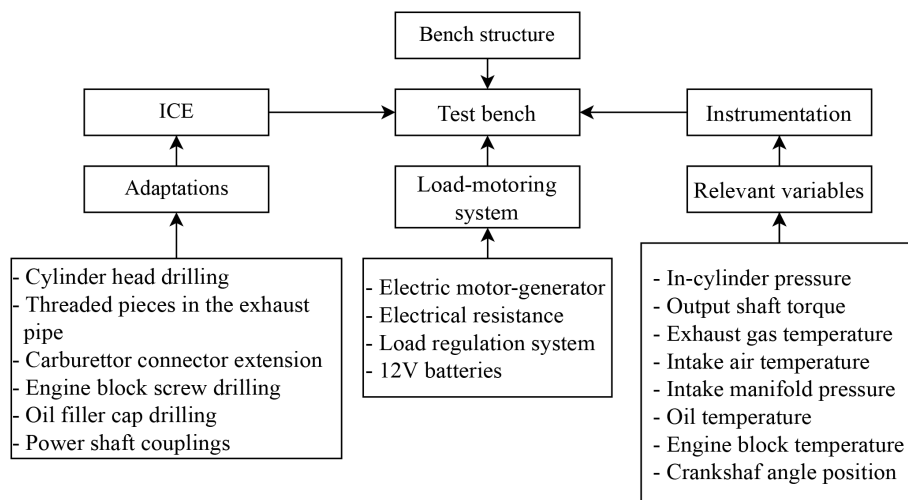


Fig. 1. Methodological scheme of the test bench integration

### 2. 2. Test bench structure

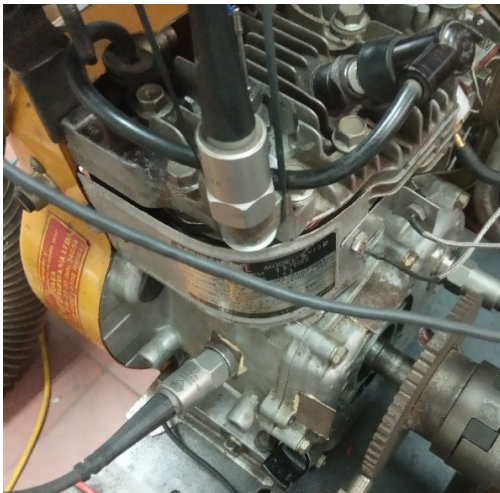
The bench structure consists of 38×5 mm steel structural angles assembled by welding. A 9.5 mm thick HR steel plate is installed on top of which the MCI and the load-motoring system are fixed, the plate is placed on four flexible supports that mitigate the vibration transmitted by the test equipment to the floor. A drawing of the described structure is shown in **Fig. 2**.



**Fig. 2.** Structure of the test bench

### 2. 3. Internal combustion engine

The Robin EY15 engine is a stationary type commonly used in air compression equipment, low flow pumps and agricultural machinery. A picture of the original engine and the technical specifications are presented in **Fig. 3**.

|   |                      |  |
|---|----------------------|--|
|  | Robin EY15           |  |
|   | Type                 | Vertical single-cylinder, side valves, spark ignited, air cooled |
|   | Bore x Stroke        | 63 mm x 46 mm  |
|   | Displacement         | 143 cm <sup>3</sup>  |
|   | Compression ratio    | 6.3:1  |
|   | Max power            | 2.6 kW at 4000 min <sup>-1</sup>                                 |
|   | Max torque           | 6.7 Nm at 2800 min <sup>-1</sup>                                 |
|   | Min fuel consumption | 380 g/kWh  |
|   | Lubrication type     | Splash   |
|   | Lubricant (Quantity) | 20W 50 (600 ml)  |
|   | Fuel system          | Horizontal carburetor  |
|   | Aspiration type      | Naturally  |
|   | Fuel                 | Gasoline   |

**Fig. 3.** Robin EY15 engine

### 2. 4. Load-motoring-starting system

The load-motoring system is composed by a permanent-magnet direct current motor-generator mechanically coupled to the ICE, an electric heating resistor equipped with an electronic load regulation system and a set of six 12 V batteries.

The motor-generator is a single device that can operate as direct starter motor, motoring device, and also can perform braking if the ICE is loaded. To operate as a load system, the MCI is ignited and drives the electric generator, the voltage delivered by the generator is proportional to the rotational speed, **Fig. 4**. The electric generator (*G*) and the electric resistor (*R*) terminals are connected to the load regulation system (*SW*), **Fig. 5**. The system (*SW*) is a 120 V powered solid state switch, which switches the generator (*G*) and the resistor (*R*) on and off in a pulsed form.

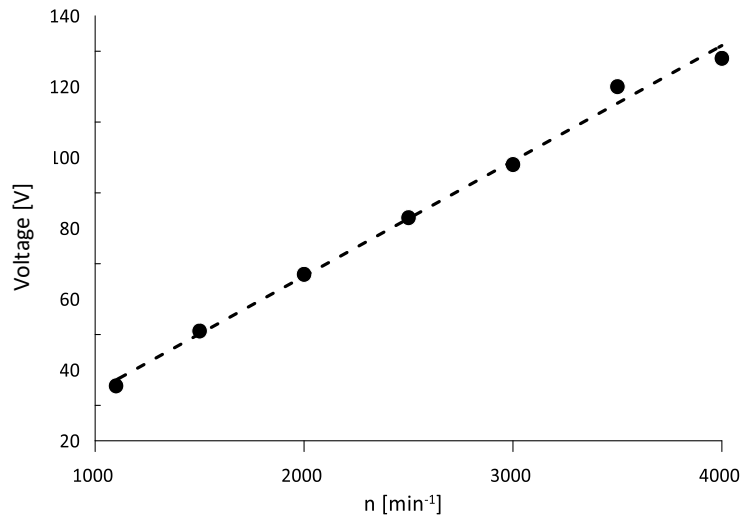


Fig. 4. Motor-generator voltage against rotation speed

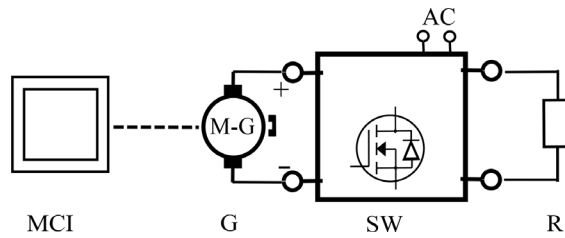


Fig. 5. Block diagram of the load system

The electrical circuit of the SW system is shown in Fig. 6.

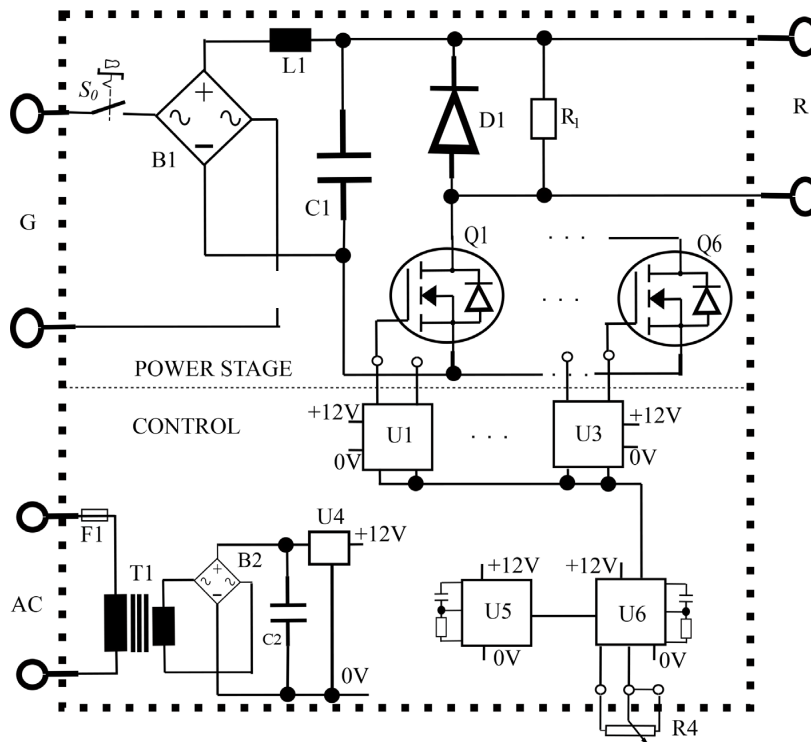
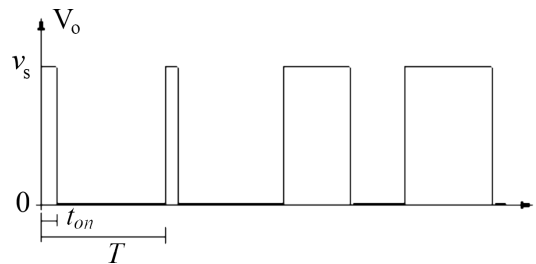


Fig. 6. Electronic Circuit of the Load Regulation System

The *SW* module is composed by a power circuit and a control circuit. In the power circuit, a single-phase rectifier consisting of *B1*, *L1* and *C1*, which ensures a filtered output voltage with fixed supply polarity of the resistor *R*. This allows the system to be used if for some reason the direction of rotation of the generator is reversed or even if it is replaced by an alternating current generator. Diode *D1* protects against transients at the output.

Commutation is achieved by six IRFP360 MOSFET transistors parallel connected (*Q1* to *Q6*), to provide commutation up to 80 A. In the control circuit, *U5* is a square wave generator circuit based on CD4047, which is transmitted to a monostable multivibrator *U6* based on CD4538, which has a rheostat *R4* to adjust the switching time duration (*ton*) shown in **Fig. 7**.



**Fig. 7.** Pulse width modulation

The six transistors (*Q1* to *Q6*) are commanded by circuits *U1* to *U3*, each one governing 2 transistors. The output signal from *U6* is fed to drivers *U1* to *U3*, to operate the transistors in the cutoff (open) or saturation (closed) condition. The square wave is adjusted in its duty cycle  $\eta$ , which is known as pulse width modulation. The duty cycle is the ratio of the on-time *t<sub>on</sub>* to the period of the square wave *T*, (1):

$$\eta = \frac{t_{on}}{T} \text{ or } \eta\% = \frac{t_{on}}{T} \times 100. \quad (1)$$

The effective voltage (*v<sub>o</sub>*) which supplies the electrical resistor (*R*) is equivalent to the product between the square root of duty cycle ( $\eta$ ) and the voltage provided by the generator (*v<sub>s</sub>*), (2). The demanded current by the resistor (*i*) is equal to the product of the square root of ( $\eta$ ) and the current that would be drawn by the electrical resistor if it were directly connected to the generator (*i<sub>max</sub>*), (3).

As the duty cycle increases, the electrical demanded current by the resistor (*R*) is higher, therefore, more electrical power will be demanded from the generator (*G*) and consequently a higher drive power will be required by the ICE:

$$v_0 = \sqrt{\eta} v_s, \quad (2)$$

$$i = \sqrt{\eta} i_{max}. \quad (3)$$

To operate as a motoring system, the electric motor is powered by 12 V batteries to drive the ICE. In this case, the rotation speed is dependent by the supply voltage, which is increased by connecting batteries, i.e., the maximum achievable rotational speed by motoring is subject to the quantity of batteries that are connected. In this case, the rotational speeds cannot be adjusted as desired, because the rotational speed depends on the number of batteries and the electrical charge of the batteries.

## 2.5 Instrumentation

The installed instruments on the test bench are presented in this section. Some of the technical characteristics are listed in **Table 1**.

The assembly of each installed instrument is shown in the following sections.

**Table 1**  
Measuring instruments of the Robin EY15 engine bench

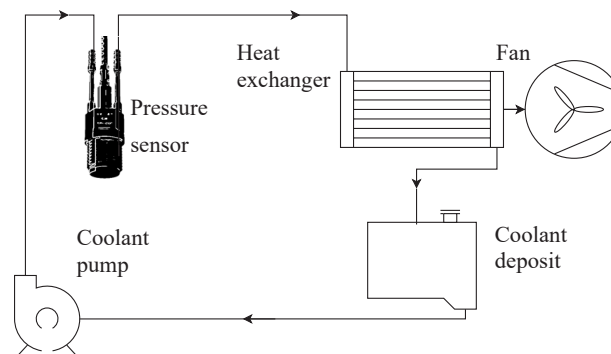
| Device                                    | Range          | Sensibility/Resolution |
|---|----------------|------------------------|
| Kistler 7061B in-cylinder pressure sensor | 0–250 bar      | –80 pC/bar             |
| Kistler 5165A charge amplifier            | 0–10 V(output) | 0.04 V/bar             |
| Futek TRS705 torque sensor with encoder   | ±50 Nm         | 0.1 V/Nm               |
| Futek IHH500 signal processor             | 0–5 V(output)  | 0.1 V/Nm               |
| Omron rotary encoder                      | 720 P/R        | 0.5°                   |
| MAP sensor                                | 10–300 kPa     | 0.053 V/kPa            |
| K type thermocouples                      | <1300 °C       | 41 μV/°C               |

### 2. 5. 1. In-cylinder pressure sensor

The in-cylinder pressure is measured by a Kistler 7061B liquid-cooled piezoelectric sensor. To install the sensor, a 14×1.25 mm threaded hole was drilled on the cylinder head. The pressure measurement chain is complemented by a Kistler 5165 A charge amplifier that processes and amplifies the transmitted signal from the pressure sensor, making it suitable to be captured by a data acquisition system, **Fig. 8**.

To avoid the overheating of the pressure sensor, a liquid cooling system composed by a low-flow rotary pump, an air heat exchanger, a fan and a coolant deposit is employed. The connected system to the pressure sensor is shown in **Fig. 9**.

|   |                              |
|---|------------------------------|
| Kistler 7061B in-cylinder pressure sensor |                              |
| Type                                      | Piezoelectric – water cooled |
| Pressure range [bar]                      | 0–250                        |
| Sensibility [pC/bar]                      | –80                          |
| Tightening torque [Nm]                    | 25                           |
| Capacitance [pF]                          | 11                           |
| Cooling water pressure [bar]              | ≤6                           |
| Kistler 5065 A charge amplifier           |                              |
| Voltage supply [V]                        | 24                           |
| Signal outputs                            | 4                            |
| Voltage output [V]                        | ±10                          |
| Sensibility [V/bar]                       | 0.04                         |
| Resolution [bits]                         | 16                           |

**Fig. 8.** In-cylinder pressure sensor, conditioning, and assembly**Fig. 9.** Pressure sensor cooling system.

### 2. 5. 2. Output Torque

The Futek TRS705 torque sensor is coupled to the ICE and motor-generator by means of flexible spider-type joints. All the shafts are aligned and fixed to the test bench structure plate, the

assembly and specifications of the meter are shown in **Fig. 10**. The sensor has an encoder which measures the shaft rotational frequency, which is equal to the crankshaft rotational speed of the Robin EY15 engine. The torque measurement chain is complemented by a Futek IHH500 data processor, which provides electrical supply to the torque sensor and the encoder, processes the torque and rotational speed signals, and shows the signals mean value on a screen. The processed torque signal is sent to a data acquisition system.



| TRS705 torque sensor                       |        |
|--|--------|
| Type                                       | Rotary |
| Voltage supply [V]                         | 11–26  |
| Voltage output [V]                         | ±5     |
| Range [Nm]                                 | ±50    |
| Sensibility [V/Nm]                         | 0.1    |
| Max rotation speed [min <sup>-1</sup> ]    | 7000   |
| Safe overloading                           | 150 %  |
| Protection                                 | IP40   |
| Encoder                                    |        |
| Voltage supply [V]                         | 5      |
| Pulses per rotation                        | 360    |
| Resolution [°]                             | 1      |
| IHH 500 processor                          |        |
| Voltage supply [V]                         | 12     |
| Voltage output to rotary torque sensor [V] | 5–24   |
| Analog output [V]                          | ±5     |
| Sensibility [V/Nm]                         | 0.1    |
| Max sampling rate [S/s]                    | 5–4800 |
| Internal resolution [bits]                 | 24     |
| Protection                                 | IP64   |

**Fig. 10.** Futek TRS705 torque sensor assembly and specifications

### 2. 5. 3. Temperatures

Four type K thermocouples are located at various sites of interest. A thermocouple is installed in the engine block using one of the fixing screws of the cooling air flow directing plate, with a concentric drilling to insert the thermocouple, ensuring electrical insulation by means of heat shrink hose and high temperature resistant acrylic (there is no direct contact between the thermocouple and the block or the screw). A longer carburetor-intake manifold connector is manufactured to fit a thermocouple exposed to the intake air. The connector is drilled to insert the thermocouple and a quick-drying glue is applied to fix the cable and seal any air leaks. The oil filler plug is drilled to insert another thermocouple which has contact with the crankcase lubricant and a glue is applied to the plug bore to prevent lubricant leakage. Finally, to measure the exhaust gases temperature, a thermocouple with a threaded cap is installed in a threaded stainless-steel cylinder which is welded to the exhaust pipe. The installation of the various thermocouples is shown in **Fig. 11**.

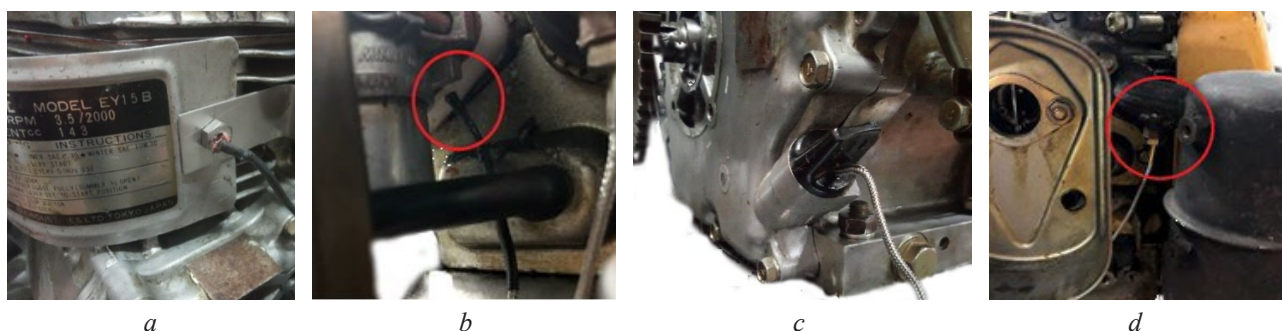


**Fig. 11.** Thermocouple installation:  
*a* – engine block; *b* – intake manifold; *c* – oil plug; *d* – exhaust pipe

### 2. 5. 4. Intake manifold pressure

To measure the pressure in the intake manifold, an additional hole is drilled in the carburetor-intake manifold connector, to fit a nipple which connects the intake manifold to the manifold pressure sensor (MAP). The sensor is a piezoresistive membrane type commonly used in vehicles with electronic injection system. The fitting and the MAP sensor are shown in Fig. 12.

The MAP sensor is characterized to find the equation of the output voltage as a function of pressure. The electrical sensor response and technical data are provided in Fig. 13.

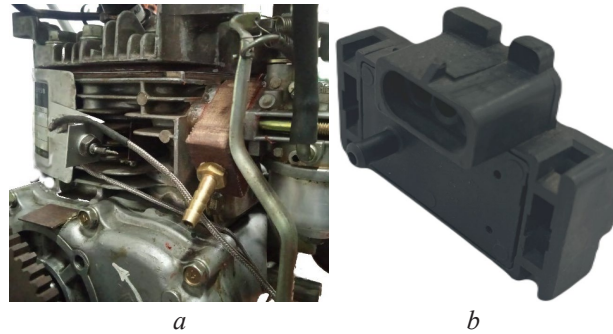


Fig. 12. MAP sensor installation:  
*a* – intake manifold connector with sensor hose nipple; *b* – MAP sensor

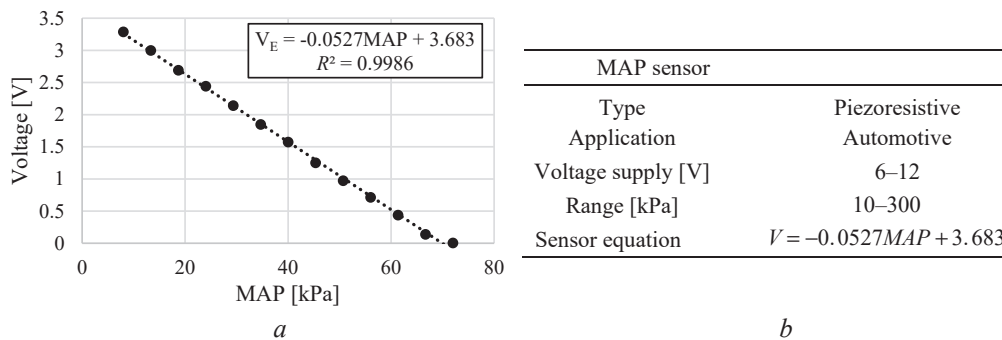


Fig. 13. MAP sensor characterization: *a* – sensor graph; *b* – sensor specifications

### 2. 5. 5. Crankshaft angle position

The crankshaft angle position can be determined by a rotary encoder mounted on the crankshaft flywheel side end or an encoder mounted on the free end of the motor-generator shaft. Each encoder provides a signal of 720 pulses for each crankshaft rotation ( $0.5^\circ$  per pulse) through one of the output channels and another channel provides a pulse for each rotation which is synchronized with the top dead center position. The encoders installation and technical data are presented in Fig. 14.

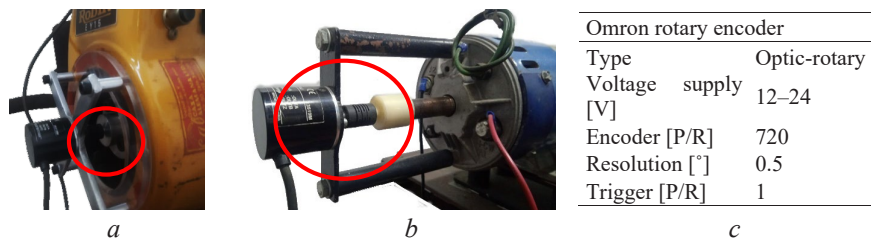


Fig. 14. Encoder installation:  
*a* – Crankshaft flywheel end; *b* – motor-generator free end; *c* – specifications

### 2. 6. Acquisition data system

This system is based on a NI 9178 chassis which has eight slots to connect different signal acquisition cards. In this work, four cards are used, one NI 9222 and one 9223 for fast signals,



one NI 9234 only for accelerometers and one 9211 dedicated to thermocouples. In order to synchronize the fast signals with the vibration signals, a sampling rate of 51200 S/s was used. In the case of the thermocouples, due to the characteristics of the acquisition card, the sampling rate had to be of 10 S/s. **Table 2** lists the components of the data acquisition system and some of their technical characteristics, including the captured variables or sensors that are connected to each card.

**Table 2**

Equipment and technical characteristics of the NI cDAQ 9178 data acquisition system

| Device       | Sampling rate | resolution    | Range    | Connected sensors or acquired signals             |
|--------------|---------------|---------------|----------|---|
| NI cDAQ 9178 | ≤500 kS/s     | 32 bits (max) | −20–25 V | Data acquisition cards                            |
| NI 9222      | ≤500 kS/s     | 16 bits       | ±10 V    | MAP, In-cylinder pressure, torque sensor, encoder |
| NI 9223      | ≤1 MS/s       | 16 bits       | ±10 V    |   |
| NI 9211      | 14 S/s        | 24 bits       | ±80 mV   | Thermocouples                                     |

## 2. 7. Methods for experimental determination of mechanical losses

In this section, two experimental methods to determine the mechanical losses of ICE are presented. The variables that are minimally measured to apply each method are mentioned and the equations for calculating the mechanical losses are also presented.

### 2. 7. 1. Indicated diagram method

This method evaluates the total mechanical losses during fired engine operation, i.e. the effects of engine speed and load on the thermal and tribological regimes under normal operating conditions can be evaluated [9, 12, 16, 22, 23]. To apply the method, it is necessary to determine the mean effective indicated pressure (IMEP) and the mean brake effective pressure (BMEP), which are necessary to determine the mean effective mechanical loss pressure (FMPE), (1).

To apply the method, the effective torque, the in-cylinder pressure and the crankshaft angle position must be measured [12, 24–26]. Using the crankshaft angle position and the piston-rod-crank mechanism geometry, the volume enclosed in the cylinder is calculated, (5). The indicated diagram, or  $P$ - $v$  diagram, is obtained by plotting the in-cylinder pressure versus the cylinder volume. The IMEP corresponds to the ratio between the work that is transmitted to the piston head during the compression and expansion processes due to the effect of combustion and the engine displacement, (6). The BMEP is the ratio between the effective work available on the engine output shaft in each cycle and the engine displacement, (7):

$$FMPE = IMEP - BMEP, \quad (4)$$

$$V_{cil} = \frac{V_d}{R_c - 1} + \frac{\pi B^2}{4} \left[ \frac{S}{2} \left( 1 - \cos \theta + \frac{S}{8L} (1 - \cos 2\theta) \right) \right], \quad (5)$$

$$IMEP = \frac{\oint P dV_{cil}}{V_d}, \quad (6)$$

$$BMEP = \frac{2\pi T}{iV_d}, \quad (7)$$

where (FMPE) is the mean effective mechanical loss pressure, (IMEP) is the mean effective indicated pressure, (BMEP) is the mean effective brake pressure, ( $V_{cil}$ ) is the cylinder volume, ( $V_d$ ) is the engine displacement, ( $\theta$ ) is the crankshaft angle position, ( $L$ ) is the connecting rod length, ( $S$ ) is the piston stroke, ( $P$ ) is the combustion chamber pressure, ( $T$ ) is the torque and ( $j$ ) is 1 for 2 T engines and 0,5 for 4 T engines.

### 2. 7. 2. Motoring method

The total power of mechanical losses, determined by the motoring method, corresponds to the power delivered by an electric motor to drive and maintain the test ICE at a constant speed [9, 25]. This method is applied in the absence of combustion, so the dynamic, thermal and tribological conditions differs from those achieved in an ignited engine [9, 12].

Measurement of the torque with which the electric motor drives the ICE is required. In this case the FMEP corresponds to the ratio between the effective drive work and the engine displacement, (7). Also, it is possible to have approximations by measuring the current and voltage in the electric motor to subsequently calculate the electrical power, (8). However, there is uncertainty in the electric motor efficiency:

$$N_{pm} = V_E I_E, \quad (8)$$

where ( $N_{pm}$ ) is the mechanical loss power, ( $V_E$ ) is the supply voltage and ( $I_E$ ) is the current.

### 2. 8. Test methodology

This section presents the engine speeds and throttle valve openings selected to determine the FMEP of the engine with each experimental method. For the firing tests, the engine is run for about three minutes to allow the lubricant temperature to stabilize. In the case of the drag tests, the engine is started for five minutes at idle speed to increase the oil temperature each time the throttle opening is changed, **Table 3**.

**Table 3**  
Test conditions

| Throttle opening | Motoring method                      | Indicated diagram method                       |
|------------------|--------------------------------------|--|
|                  | Rotation speed [ $\text{min}^{-1}$ ] |  |
| 0 %              | 600, 900, 1250, 1550, 1900           | No tested                                      |
| 25 %             | 600, 900, 1200, 1500, 1750           | 1500, 1900, 2500, 2800                         |
| 50 %             | 600, 900, 1200, 1500, 1700           | 1500, 2000, 2900, 3100, 3550, 4150, 4450, 4800 |
| 75 %             | 600, 900, 1200, 1500, 1700           | No tested                                      |
| 100 %            | 600, 900, 1200, 1500, 1600, 1900     | 2100, 3500, 4200, 4450, 4800                   |

## 3. Results and discussion

**Fig. 15** shows the in-cylinder pressure, the torque on the output shaft and the intake manifold pressure curves referred to the crankshaft angle position under motoring and fired conditions at an engine speed of  $1500 \text{ min}^{-1}$  and 50 % throttle valve opening. The in-cylinder pressure reaches up to about 7.45 bar in motoring conditions, and about 17 bar in fired conditions due to the contribution of the combustion process. The gas load due to combustion causes the torque at the output shaft to reach up to around 26.3 Nm.

**Fig. 16** shows the in-cylinder pressure versus volume diagrams in motoring and fired conditions. It can be seen that due to the combustion process, the work generated during the expansion stroke is greater than that invested in overcoming the compression of the engine, so that there is surplus work (indicated work) that is partially transformable into useful work. When the engine is motored, the expansion work is less than the compression work due to leakage and heat losses.

**Fig. 17** shows the temperature maps of intake air, oil, engine block and exhaust gases during the tests in fired conditions. It can be seen that the intake air temperature decreases as engine speed increases, varying between  $28 \text{ }^\circ\text{C}$  at  $1500 \text{ min}^{-1}$  and around  $21 \text{ }^\circ\text{C}$  at  $4800 \text{ min}^{-1}$ , while the oil, engine block and exhaust gas temperatures increase as engine speed and load increases, varying between  $80\text{--}118 \text{ }^\circ\text{C}$ ,  $107\text{--}159 \text{ }^\circ\text{C}$  and  $237\text{--}483 \text{ }^\circ\text{C}$ , respectively. A map of the lubricant

temperature in the motoring tests is also presented, which shows that for engine speeds close to  $600 \text{ min}^{-1}$  it varies between  $56\text{--}65 \text{ }^\circ\text{C}$ , due to the pre-heating of the engine. However, as the engine speed increases, the oil temperature decreases to around  $43 \text{ }^\circ\text{C}$  at higher speeds, due to the air-cooling system operation.

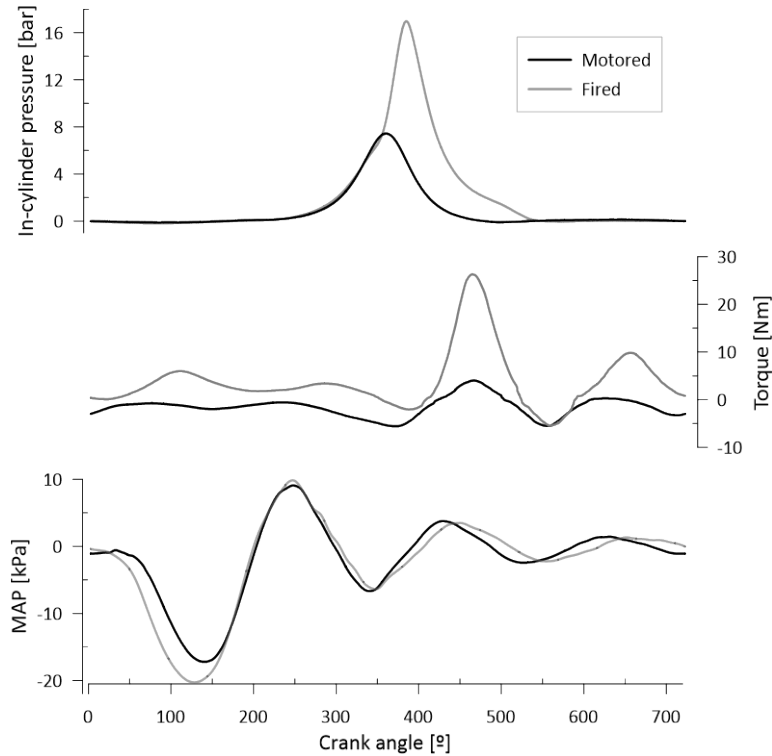


**Fig. 15.** Cylinder pressure, torque and intake pressure curves versus angular position at  $1500 \text{ min}^{-1}$  and 50 % throttle opening

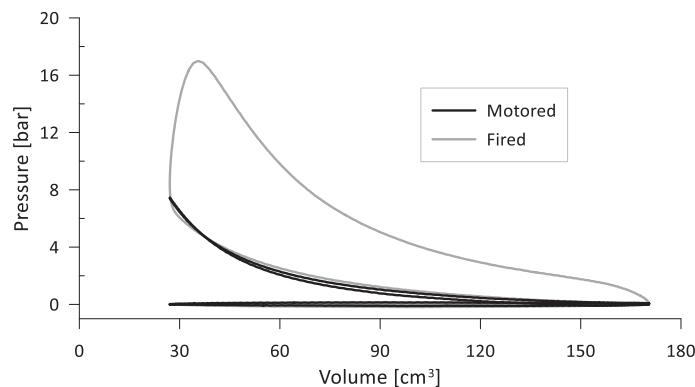


**Fig. 16.** Indicated diagrams at  $1500 \text{ min}^{-1}$  and 50 % throttle opening

**Fig. 18** shows the *FMEP* plotted against speed and throttle valve openings. The results of the *FMEP* in motoring conditions show that increasing the valve opening leads to decreases in the *FMEP*, where for a throttle opening of 0 %, the *FMEP* varies between  $1.08\text{--}1.51 \text{ bar}$  and at 100 % opening the *FMEP* varies between  $0.97\text{--}1.35 \text{ bar}$ . This is due to a reduction of the air flow restriction through the intake duct when the throttle opening increases. It can be observed that the *FMEP* increases with increasing engine speed because the coefficient of friction increases under the hydrodynamic lubrication regime. These results are close to the *FMEP* reported by [27, 28] for motorcycle engines tested in motoring conditions.

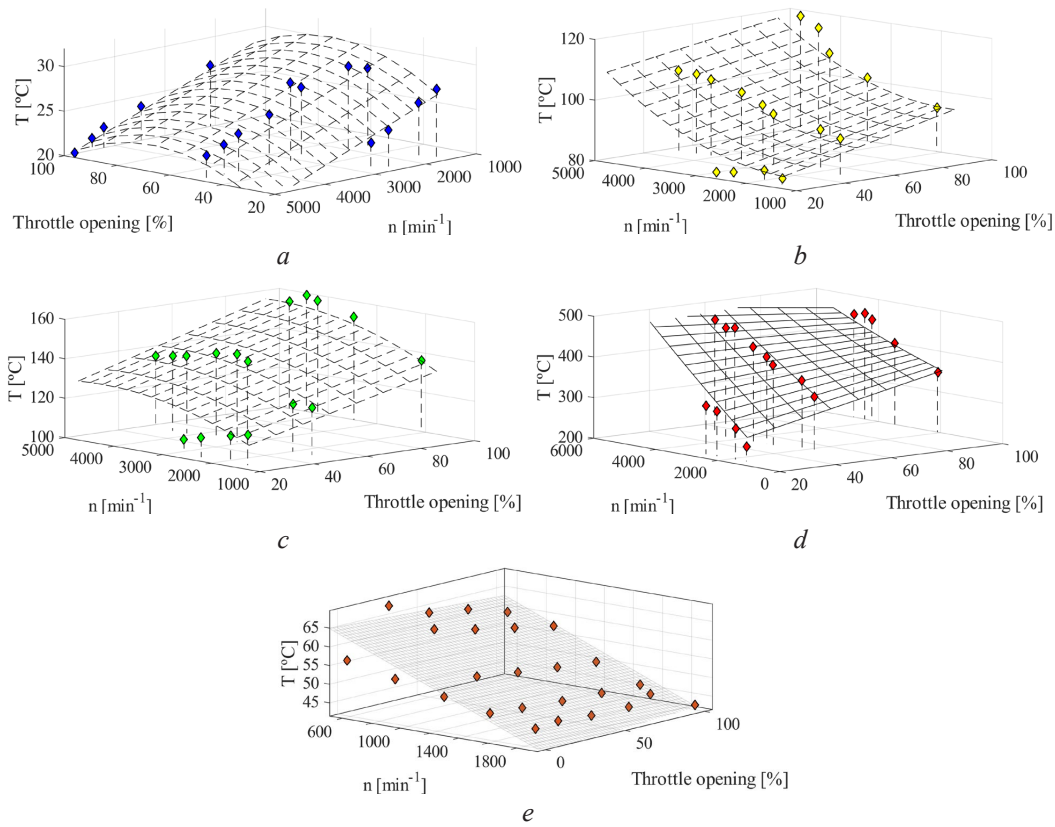


**Fig. 17.** Temperature surface maps:  
*a* – intake; *b* – lubricant; *c* – engine block; *d* – exhaust and *e* – lubricant in motoring conditions

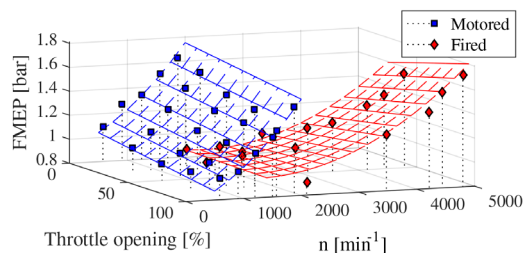


**Fig. 18.** FMEP comparison of the Robin engine by the indicated diagram and motoring methods

It can be observed that the *FMEP* for fired engine tests increases mainly with increasing rotational speed, however, it has a slight increase with higher loads, influenced by the combustion gas pressure, which causes an increase in the contact forces between the cylinder and the crank-slider mechanism, varying between 0.82 bar at 1900  $\text{min}^{-1}$  and 1.13 bar at 2800  $\text{min}^{-1}$  at 25 % load and between 0.91 bar at 2100  $\text{min}^{-1}$  and 1.73 bar at 4800  $\text{min}^{-1}$  at 100 % load. The behaviour of the *FMEP* with load increment agrees with the results reported by [29] for a four-cylinder spark ignition engine at 1600  $\text{min}^{-1}$ .

Comparing the *FMEP* determined by means of the indicated diagram and the motoring methods, it is obtained that the mechanical losses in motoring are greater with percentage differences between 52.3 % and 90.1 % at 25 % throttle opening and between 27.9 % and 52.8 % at 50 % throttle opening for rotational speeds between 1500  $\text{min}^{-1}$  and 2000  $\text{min}^{-1}$ , taking as a reference the *FMEP* results determined by means of the indicated diagram method. This behaviour is caused by the high viscosity of the lubricant in the motoring tests, which are carried out in the absence of combustion, as the oil is not heated, and the lower loads on the mechanisms due to the combustion process absence, causing that the friction coefficient in the kinematic pairs that operate under

the hydrodynamic lubrication regime increases. This behaviour is in accordance with [16], where the FMEP in motoring conditions is higher than that of the fired conditions. However, the maximum difference is 15 % between motoring and fired engine mechanical losses, which is lower than the differences found for the Robin engine. It is noted that in this work there is a significant difference in oil temperature between the motoring and fired tests.

As a sought outcome of the experimental work conducted on the developed test bench, (9), (10) are empirical correlations that correspond to the trend surfaces of the  $FMEP$  data in Fig. 18;  $FMEP_M$  and  $FMEP_F$  are the mean effective pressure of mechanical losses in motored and fired engine respectively, ( $n$ ) is the rotational speed in  $\text{min}^{-1}$  and ( $T_{op}$ ) is the throttle valve opening percentage.

The equations presented are particular for the Robin EY15 engine, so they must be calibrated in order to calculate the  $FMEP$  for other engines.

$$FMEP_M = 6.42 \times 10^{-8} n^2 - 2.57 \times 10^{-4} n + 9 \times 10^{-7} n T_{op} - 1.49 \times 10^{-3} T_{op} + 1.2, R^2 = 0.97, \quad (9)$$

$$FMEP_F = 1.17 \times 10^{-7} n^2 + 1.82 \times 10^{-4} n + 1.07 \times 10^{-7} n T_{op} - 1.74 \times 10^{-3} T_{op} + 0.92, R^2 = 0.96. \quad (10)$$

Finally, it should be remembered that, when using a battery for internal combustion engine motoring, the speed range is limited by the number of batteries and the electrical charge. In this case, it was only possible to test up to a rotational speed of  $1900 \text{ min}^{-1}$ . Although the electronic load regulation system can be used as a source for the electric motor in motoring mode, the safe electrical current that the system can provide is not enough to drive the Robin EY15 engine.

An additional limitation of the motoring tests is related to the lubricant temperature, which is not controlled and always is lower than the oil temperature of fired engine conditions. Due to the temperature difference in the tests, viscosity variations of the oil are expected, causing differences in the FMEP results.

#### 4. Conclusions

A test bench was integrated to experimentally determine the mechanical losses of small single-cylinder internal combustion engines. The bench was equipped with a proprietary controlled electronic load-motoring system consisting of a permanent-magnet motor-generator, a charge regulator and a set of batteries. Special attention has been paid to the development of the electronic circuit of the load regulation system ( $SW$ ), to be operated from  $120 \text{ V AC}$  to provide electrical power to the permanent-magnet motor-generator and make it a variable speed starter motor or motoring device. Since, the circuit overheated due to high peaks of torque demand in some crankshaft angles in direct starting and motoring conditions, it was decided to be conservative and use groups of batteries for starting or motoring. The electronic circuit of load regulation withstood better operating in load mode. Making room for improvement, it is envisaged to modify the control strategy of the electronic circuit for starting and motoring conditions to provide more starting current.

The bench instrumentation includes transducers for in-cylinder pressure, output shaft torque, intake air pressure, crankshaft angle position and temperatures of intake air, lubricant, engine block and exhaust gases, together with a data acquisition system with a sampling rate of up to  $1 \text{ MS/s}$  was used. The in-cylinder pressure, torque and MAP signals captured in motoring and fired engine were compared, allowing to observe the difference in the loads over the piston head and on the output shaft caused by the combustion. It was possible to follow the growth of lubricant, engine block and exhaust gas temperatures as engine speed and load increased.

Two mechanical loss determination methods (motoring method and indicated diagram method) were applied to a single-cylinder spark ignition Robin EY15 engine. It was obtained that the FMEP by the motoring method varies between  $0.97\text{--}1.51 \text{ bar}$  and between  $0.82\text{--}1.73 \text{ bar}$  by the indicated diagram method. It is observed that under comparable engine speeds and throttle openings, the FMEP measured in motoring is between  $27.9\text{--}90.1 \%$  higher than that measured with the fired engine, attributable to the lower lubricant temperature in the motoring tests, i.e. higher viscosity, and the lower loads on the engine mechanisms, so the friction coefficient under

the hydrodynamic lubrication regime is higher, causing a greater mechanical work to be invested to overcome the engine friction.

Two empirical correlations, very useful in the modelling of the engine tested, adjusted to the experimental data are provided to determine the mechanical losses of the Robin EY15 engine.

#### **Conflict of interest**

The authors declare that they have no conflict of interest in relation to this research, whether financial, personal, authorship or otherwise, that could affect the research and its results presented in this paper.

#### **Financing**

The study was performed without financial support.

#### **Data availability**

Data will be made available on reasonable request.

#### **Acknowledgment**

The authors thank the Universidad Tecnológica de Pereira UTP (Technological University of Pereira) for their support throughout the research.

#### **Use of artificial intelligence**

The authors confirm that they did not use artificial intelligence technologies when creating the current work.

---

#### **References**

- [1] Romero P, C. A., Henao Castañeda, E. D. J., Monroy Jaramillo, M., Pérez Castro, W. (2016). Diseño y construcción de un banco de pruebas de motores para ensayos de investigación formativa. In II Jornadas Iberoamericanas de Motores Térmicos y Lubricación (MTL 2016), 333–344. Available at: <http://sedici.unlp.edu.ar/handle/10915/77544>
- [2] Freschi, M., Paniz, A., Cerqueni, E., Colella, G., Dotelli, G. (2022). The Twelve Principles of Green Tribology: Studies, Research, and Case Studies – A Brief Anthology. *Lubricants*, 10 (6), 129. doi: <https://doi.org/10.3390/lubricants10060129>
- [3] Narváez Pallares, H., Villareal Acosta, S., Duarte Forero, J., Rincón Montenegro, A. (2017). Implementación de un banco para pruebas en motor Diésel monocilíndrico con aplicaciones investigativas. *Sci. Tech.*, 22 (4), 330–340. Available at: <https://www.redalyc.org/pdf/849/84955649005.pdf>
- [4] Menon, S., Moulton, N., Cadou, C. (2007). Development of a Dynamometer for Measuring Small Internal-Combustion Engine Performance. *Journal of Propulsion and Power*, 23 (1), 194–202. doi: <https://doi.org/10.2514/1.19825>
- [5] Ausserer, J. K., Litke, P. J., Groenewegen, J.-R., Rowton, A., Polanka, M., Grinstead, K. (2013). Development of Test Bench and Characterization of Performance in Small Internal Combustion Engines. SAE International. doi: <https://doi.org/10.4271/2013-32-9036>
- [6] Ramírez, J. D., Mejía Hernández, J. C., Quintero, H. F., Henao Castañeda, E. D. J., Romero Piedrahita, C. A., Pérez Castro, W. (2019). Banco de instrumentación para el acondicionamiento y adquisición de señales provenientes de un motor de combustión interna. *Revista Colombiana De Tecnologías De Avanzada (RCTA)*. doi: <https://doi.org/10.24054/16927257.v0.n0.2018.3300>
- [7] Henao Castañeda, E. D. J., Romero Piedrahita, C. A., Quintero, H. F., Mejía, J. C., Ramírez Alzate, J. D. (2021). Diseño, construcción e instrumentación de un banco de pruebas para caracterización de pérdidas mecánicas en motores de encendido por chispa de bajas potencias. In *Apropiación social del conocimiento investigación, innovación y extensión*, 426–465.
- [8] Kumar, V., Sinha, S. K., Agarwal, A. K. (2018). Tribological Studies of an Internal Combustion Engine. *Energy, Environment, and Sustainability*, 237–253. doi: [https://doi.org/10.1007/978-981-13-3275-3\\_12](https://doi.org/10.1007/978-981-13-3275-3_12)
- [9] Noorman, M. T., Assanis, D. N., Patterson, D. J., Tung, S. C., Tseregounis, S. I. (2000). Overview of Techniques for Measuring Friction Using Bench Tests and Fired Engines. SAE Technical Paper Series. doi: <https://doi.org/10.4271/2000-01-1780>
- [10] Tormos, B., Ramírez, L., Johansson, J., Björling, M., Larsson, R. (2017). Fuel consumption and friction benefits of low viscosity engine oils for heavy duty applications. *Tribology International*, 110, 23–34. doi: <https://doi.org/10.1016/j.triboint.2017.02.007>
- [11] Monieta, J. (2022). Method and a Device for Testing the Friction Force in Precision Pairs of Injection Apparatus of the Self-Ignition Engines. *Energies*, 15 (19), 6898. doi: <https://doi.org/10.3390/en15196898>
- [12] Koch, F., Geiger, U., Hermsen, F.-G. (1996). PIFFO – Piston Friction Force Measurements During Engine Operation. SAE Technical Paper Series. doi: <https://doi.org/10.4271/960306>

- [13] Romero-Piedrahita, C., Rodríguez-Valencia, A., Monroy-Jaramillo, M. (2020). Ensamble e instrumentación de un banco didáctico para pruebas de arranque en motores de combustión interna. *Revista UIS Ingenierías*, 19 (3), 37–48. doi: <https://doi.org/10.18273/revuin.v19n3-2020004>
- [14] Romero, C. A., Henao Castañeda, E. de J. (2019). Developing Small Variable Compression Ratio Engines for Teaching Purposes in an Undergraduate Program. *SAE Technical Paper Series*. doi: <https://doi.org/10.4271/2019-01-0331>
- [15] Fang, C., Meng, X., Xie, Y., Wen, C., Liu, R. (2019). An improved technique for measuring piston-assembly friction and comparative analysis with numerical simulations: Under motored condition. *Mechanical Systems and Signal Processing*, 115, 657–676. doi: <https://doi.org/10.1016/j.ymssp.2018.06.015>
- [16] Heywood, J. B. (1988). *Internal Combustion Engine Fundamentals*. McGraw Hill.
- [17] Caruana, C., Farrugia, M., Sammut, G., Pipitone, E. (2019). Further Experimental Investigation of Motored Engine Friction Using Shunt Pipe Method. *SAE International Journal of Advances and Current Practices in Mobility*, 1 (4), 1444–1453. doi: <https://doi.org/10.4271/2019-01-0930>
- [18] Caruana, C., Farrugia, M., Sammut, G. (2018). The Determination of Motored Engine Friction by Use of Pressurized ‘Shunt’ Pipe between Exhaust and Intake Manifolds. *SAE Technical Paper Series*. doi: <https://doi.org/10.4271/2018-01-0121>
- [19] Romero, C., Henao, E., Ramirez, J. (2021). Experimental study of mechanical losses of single-cylinder spark-ignited engine. *Diagnostyka*, 22 (3), 12–24. doi: <https://doi.org/10.29354/diag/141226>
- [20] Romero, C. A., Ramírez, J. D., Henao Castañeda, E. de J. (2023). Experimental Characterization of the Mechanical Loss Components of a Single-Cylinder Spark-Ignition Engine by Progressive Disassembly Method. *SAE Technical Paper Series*. doi: <https://doi.org/10.4271/2023-01-0416>
- [21] Knauder, C., Allmaier, H., Sander, D. E., Sams, T. (2019). Investigations of the Friction Losses of Different Engine Concepts. Part 1: A Combined Approach for Applying Subassembly-Resolved Friction Loss Analysis on a Modern Passenger-Car Diesel Engine. *Lubricants*, 7 (5), 39. doi: <https://doi.org/10.3390/lubricants7050039>
- [22] Iniesta, E. (2016). Estudio y validación de una metodología de ensayo para el análisis experimental de la fuerza de fricción en el bloque pistón-camisa-segmentos de un MCI. Universidad Politécnica de Valencia. Available at: <https://m.riunet.upv.es/bitstream/handle/10251/67302/INIESTA%20-%20Estudio%20y%20validaci%3%b3n%20de%20una%20metodolog%3%a-da%20de%20ensayo%20para%20el%20an%3%a1lisis%20experimental%20de%20la%20f....pdf?sequence=2&isAllowed=y>
- [23] Levickis, D., Gailis, M., Rudzitis, J., Kreicbergs, J. (2019). Evaluation of methodology for determination of mechanical efficiency of spark ignition engine. *Engineering for Rural Development*. doi: <https://doi.org/10.22616/erdev2019.18.n300>
- [24] Skjoedt, M., Butts, R., Assanis, D. N., Bohac, S. V. (2008). Effects of oil properties on spark-ignition gasoline engine friction. *Tribology International*, 41 (6), 556–563. doi: <https://doi.org/10.1016/j.triboint.2007.12.001>
- [25] Cruz-Peragón, F., Palomar, J. M., Díaz, F. A., Jiménez-Espadafor, F. J. (2010). Fast on-line identification of instantaneous mechanical losses in internal combustion engines. *Mechanical Systems and Signal Processing*, 24 (1), 267–280. doi: <https://doi.org/10.1016/j.ymssp.2009.06.009>
- [26] Sgroi, M. F., Asti, M., Gili, F., Deorsola, F. A., Bensaid, S., Fino, D. et al. (2017). Engine bench and road testing of an engine oil containing MoS<sub>2</sub> particles as nano-additive for friction reduction. *Tribology International*, 105, 317–325. doi: <https://doi.org/10.1016/j.triboint.2016.10.013>
- [27] Yagi, S., Ishibasi, Y., Sono, H. (1990). Experimental Analysis of Total Engine Friction in Four Stroke S. I. Engines. *SAE Technical Paper Series*. doi: <https://doi.org/10.4271/900223>
- [28] Fujii, I., Yagi, S., Sono, H., Kamiya, H. (1988). Total Engine Friction in Four Stroke S.I. Motorcycle Engine. *SAE Technical Paper Series*. doi: <https://doi.org/10.4271/880268>
- [29] Gish, R. E., McCullough, J. D., Retzliff, J. B., Mueller, H. T. (1958). Determination of true engine friction. *SAE Technical Paper Series*. doi: <https://doi.org/10.4271/580063>

Received date 07.04.2023

Accepted date 10.11.2023

Published date 30.11.2023

© The Author(s) 2023

This is an open access article  
under the Creative Commons CC BY license

**How to cite:** Romero Piedrahita, C. A., Monroy Jaramillo, M., Ramírez Alzate, J. D. (2023). Test bench development and implementation for experimental determination of mechanical losses in single cylinder internal combustion engines. *EUREKA: Physics and Engineering*, 6, 78–92. doi: <https://doi.org/10.21303/2461-4262.2023.002847>